



UNIVERSITY OF LEEDS

This is a repository copy of *Characterisation of spectroscopic and magneto-optical faraday rotation in Mn²⁺- doped CdS quantum dots in a silicate glass*.

White Rose Research Online URL for this paper:
<http://eprints.whiterose.ac.uk/152678/>

Version: Accepted Version

Article:

Panmand, RP, Tekale, SP, Daware, KD et al. (3 more authors) (2020) Characterisation of spectroscopic and magneto-optical faraday rotation in Mn²⁺- doped CdS quantum dots in a silicate glass. *Journal of Alloys and Compounds*, 817. 152696. ISSN 0925-8388

<https://doi.org/10.1016/j.jallcom.2019.152696>

© 2019, Published by Elsevier B.V. This manuscript version is made available under the CC-BY-NC-ND 4.0 license <http://creativecommons.org/licenses/by-nc-nd/4.0/>.

Reuse

This article is distributed under the terms of the Creative Commons Attribution-NonCommercial-NoDerivs (CC BY-NC-ND) licence. This licence only allows you to download this work and share it with others as long as you credit the authors, but you can't change the article in any way or use it commercially. More information and the full terms of the licence here: <https://creativecommons.org/licenses/>

Takedown

If you consider content in White Rose Research Online to be in breach of UK law, please notify us by emailing eprints@whiterose.ac.uk including the URL of the record and the reason for the withdrawal request.



eprints@whiterose.ac.uk
<https://eprints.whiterose.ac.uk/>

Characterisation of spectroscopic and magneto-optical Faraday rotation in Mn²⁺-doped CdS quantum dots in a silicate glass

Rajendra P. Panmand¹, Shashikant P. Tekale¹, Krishna D. Daware², Suresh W. Gosavi², Animesh Jha^{3*} and Bharat B. Kale^{1**}

¹Center for Materials for Electronics Technology (C-MET), Ministry of Electronics and Information Technology (MeitY), Off Pashan Road, Panchawati, Pune-411008, India.

²Department of Physics, Savitribai Phule Pune University (SPPU), Pune -411007, India.

³School of Chemical and Process Engineering, University of Leeds, Leeds LS2 9JT, U.K.

ABSTRACT

We demonstrate the control of CdS and Mn²⁺-doped-CdS Q-dots in a silicate glass for magneto-optical applications. The microstructural properties of Q-dot glasses were investigated by X-Ray diffraction (XRD), Field Emission Transmission Electron Microscopy (FETEM) and the optical properties by UV-Visible-NIR and Photoluminescence (PL) spectroscopic techniques, respectively. The FETEM of the CdS QD-glass heat treated at 600°C reveals that the size of CdS and Mn²⁺-doped CdS Q-dots are in the range of 4-5 nm and 5-6nm, respectively. The observed size distributions of Q-dots were in reasonable agreement with the data, derived from X-ray line broadening and estimated average Bohr radii using the UV-visible absorption data. Photoluminescence characteristics were investigated at room temperature by exciting the CdS and Mn²⁺-doped-CdS Q-dot glasses with a 420 nm excitation source, which yielded broad emission spectra in the visible and near-IR range (450-800nm). We observed a red shift in the emission peak with increase in the Q-dot size, controlled by heat treatment temperature range (550-600°C). The room-temperature magneto-optical Faraday rotation measurements on Q-dots glasses were carried out using magnetic field strength up to 360 mT, and observed an increase in the value of Verdet constant, from 6.2 to 12.0 degree/T-cm, when comparing undoped CdS-Q-dot glass with Mn²⁺-doped CdS glass. The demonstration of enhanced Verdet constant in Q-dot silicate glasses with sub-Tesla field paves the path for engineering range magneto-optical devices for photonics, spintronics and sensors applications, in which the polarisation of photons may be controlled with low-intensity magnetic field in optical waveguides.

Keywords

Quantum dots CdS, Dichalcogenide dopant, Magento-optics glass, Faraday rotation, Photoluminescence.

1 Introduction

Dilute or semi-magnetic semiconductor (DMS) nanocrystals (NCs) are material in which impurity ions, for example, the Mn^{2+} ions replace Cd^{2+} ions in diamond and wurtzite structures. The chemical composition of the DMS-NCs is represented by $\text{A}_{1-x}\text{Mn}_x\text{B}$, where x denotes the fraction of impurity ions substitution in the DMS lattice structure [1]. The control of spectroscopic and magnetic properties of Mn^{2+} -doped group IIB (Zn, Cd, Pb) family of DMS-NCs was originally reported by controlling the size distribution at nanoscale, for offering potential applications in quantum computing, spintronics, medicine, and magneto-optics [2]. In this context, the Mn^{2+} -doped semiconductor quantum dots [3] have attracted particular attention due to the strong dependence of the electronic exchange interaction in the IIB CdS structure [4] via $[\text{Ar}]3s^23p^4(\text{S})-[\text{Ar}]4s^23d^5(\text{Mn})$, arising from the transition metal ion doping [5]. The formation of Mn-S bonds within the IIB-S structure further increases the energy of the three remaining 3d-electrons in Mn^{2+} -ion. In the absence of Mn^{2+} -ions, the structure of IIB semiconductor sulphides involves the interaction of $3p^4$ sulphur electrons interacting with completely filled d-shells of IIB metal structure ($3d^{10}$ in Zn and Cd, $5d^{10}$ in Pb). For magneto-optic applications, the control of quantum dot size distribution within the glass structure is an essential step for maintaining the optical transparency of such materials for photonic devices. However, since the nucleation and growth of Q-dots are stochastic of nature, the regime of controlled and anisotropic growth of DMS-NCs for efficient Faraday rotation remains a formidable challenge even in epitaxial controlled molecular beam techniques.

A majority of commercially available bulk magneto-optical devices are based on yttrium iron-garnet (YIG) [6] and Terbium Gallium garnets (TGG) [7], with high transparency in the visible, near-IR region and these garnet materials [8] have large Verdet constant (71.81 degree/T-cm). By comparison, the single crystal planar optical isolators are difficult to grow, especially by aligning the optical axis with the crystal growth direct. Such materials also require careful optical alignment because of the anisotropic refractive index differences, which then introduces modal mismatch. However, a number of birefringence controlled single and photonic crystal fibre optic devices are well established for the long-

haul, access and local area communication networks [9]. However, the main challenge still remains in the area of coherent and secure data transmission throughout the network, where a planarized MO-device may be able to play much more significant roles in providing a bifunctional role in a single device by controlling polarisation phase amplification of signals after optical switching, thereby providing an opportunity for a device with loss-less phase amplification. Although, both the phase amplification and optical switching are possible in the photonic crystal and standard optical fibre geometries [10], such geometries are only physically compatible with the optical fibre interconnects and, therefore, such devices are not suitable for integration with planar circuits. By contrast, a glass-based QD structures for planar magneto-optical devices may be able to play an important role. As of now, the development in MO glasses is limited because of a comparatively small Verdet constant [11-14] in spite of the fact that there has been a significant progress in the design of novel magneto-active glasses in recent years. Since, the degree of Faraday rotation (polarization), essential for optical switching and phase amplification, depends on the product of the Verdet constant (V) and the optical path-length (L), a magneto-optically transparent materials with large Verdet constant in waveguide geometries will be able to offer much better option in terms of loss-less switching with phase amplification. The nature of glass materials and its processing for optimising the nucleation and growth of quantum dots for enhancing Verdet constant particularly matters for waveguide geometries, when comparing the processing of single crystalline and polycrystalline materials which are hard to fabricate with low scattering loss and cost. For engineering the Q-dot based MO devices using glass may be possible by combining the glass fabrication with thermal annealing as a first step for engineering an MO host material with large Verdet constant.

Considering the need for optically transparent devices for phase amplification and loss-less optical switching in the secure data transmission network, we propose the use of dilute magnetic semiconductor (DMS) in a suitable glass matrix for optical integration. Although there are reports on dispersion of DMS nanocrystals in the polymer matrix (PVP) [15], however such polymers offer only 30% optical transparency in the optical window 1500-1530 nm [16], compared with close to 99.9% transparency in

pure silica. There are reports on thermal annealing and control of size distributions of the DMS Q-dots (ZnMnS [17], PbMn(Te,S) [18] CdMnTe [19] and Mn²⁺-doped Bi₂S₃ [5,20]) in oxide glass matrices, which form the basis for developing an approach for controlling the thermal annealing condition for Q-dot size distribution for Mn²⁺-doped CdS glasses. Techniques of Q-dot structural characterisation for maximizing the Verdet constant using the electron paramagnetic resonance, room temperature and below 4K magnetic susceptibility and AC field-induced magnetisation characterisation have been reported [1, 21].

In this article, an alternative method of synthesizing the DMS-NC has been explored. The CdS and Cd_{1-x}Mn_xS Q-dots in a glass matrix, were grown using the glass melting followed by controlled heat treatment. The X-ray diffraction, Field-emission transmission electron microscopy (FE-TEM) and photoluminescence (PL) characterization techniques were adopted for engineering such materials for potential device applications. Besides controlling and optimizing the Verdet constant in Mn²⁺-doped CdS glass in a silicate glass, we also report the QD size distribution dependence of Verdet constant, by controlling annealing.

2 Experimental details

The glass samples with DMS-QD were prepared with the nearly 99.9 % purity synthetic precursors (Sigma–Aldrich). The host glass matrix for the quantum dot growth was constituted of a nominal composition (mol %): 50-52SiO₂–6B₂O₃– 8-10ZnO– 12K₂O – 10Na₂O – 6MgO – 4TiO₂. The composition was melted and homogenized at 1150°C for 4 hours in nitrogen atmosphere using an alumina crucible. For making and comparing the spectroscopic and MO properties CdS-doped silicate glass with Mn²⁺-doped CdS glass, 2 mol% CdS and Cd_{0.844}Mn_{0.166}S, were incorporated, respectively, in each homogenized silicate melt. The doping concentration of each was calculated a priori, based on the evidences presented in relevant literature [1,5,7,8,21-23]. After doping the melts with CdS and Cd_{0.844}Mn_{0.166}S, they were quenched in air in a stainless steel mould. After casting the CdS-containing semiconductor glass samples, isothermal annealing treatments for 8 hours were carried out in the

temperature range of 550-600°C for controlling the growth of DMS quantum dots. The transmission electron microscopic characterization was carried out using a field emission source in a Philips CM20 (300 kV) microscope. The structural and phase analysis was carried out using the X-Ray Diffractometer (XRD) (Bruker D8). However, for characterizing the UV-visible-NIR absorption properties of Q-dot doped glass samples before and after annealing, the Perkin Elmer Lambda 950 spectrophotometer was used. The photoluminescence (PL) measurements were performed with an excitation source at 420 nm using a Horiba Fluorolog 3 Fluorimeter. For magneto-optical Faraday rotation characterisations of CdS and Mn²⁺-doped quantum dots glass, each 1-mm thick sample was optically polished with parallel face, and the polarisation rotation of laser beam was recorded using a phase sensitive detection technique, as discussed previously [24]. Fig. 1 shows the ray diagram of optical setup used for magneto-optical Faraday rotation (MOFR) characterisation in Q-dot containing CdS and Mn²⁺-doped CdS glass samples. The MOFR study was carried out in magnetic field ranging from 40 to 360 mT. The diode lasers with 35 mW output powers operating at 405, 532, 635 and 670 nm wavelength were selected for the MOFR characterisation.

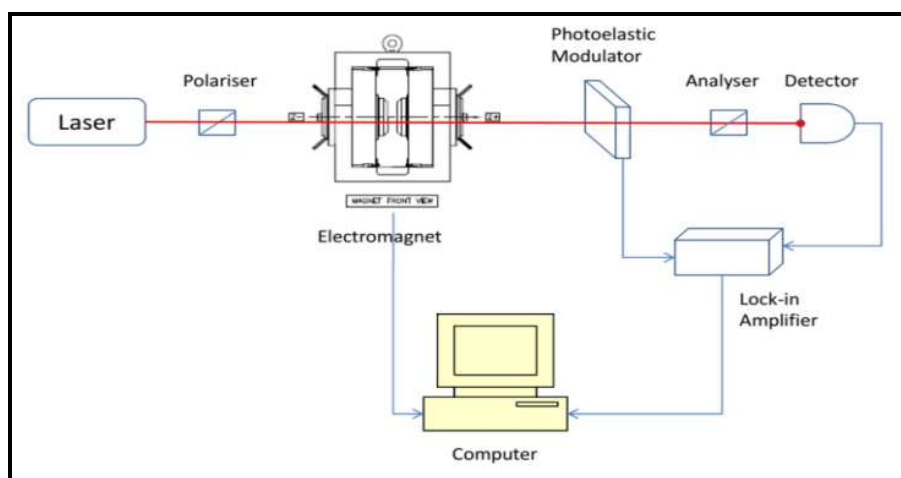


Fig.1: The ray diagram of optical setup used for the MOFR characterisation of CdS and Mn²⁺-doped CdS containing Q-dot silicate glasses.

3 Results and discussion

The X-ray powder diffraction (XRD) of heat treated DMS-QD glass was carried out by scanning glass powder samples at a scan speed 0.58° per minute. From the diffractogram in Fig. 2, the presence of broad peak shows the evidence for the presence of amorphous silicate matrix, depicted by the large and broad peak on to which the diffraction peaks of nano crystallites of CdS and Mn^{2+} -doped CdS are apparent. The d-spacing data from diffraction analysis are in good agreement with the JCPD data (77-2306) for the hexagonal CdS. From the diffraction analysis, it is possible to confirm the presence of nano-crystalline Q-dots of CdS and Mn^{2+} -doped CdS, which have formed as a result of thermal annealing for 8 hours at 550°C and 600°C . The crystallite size range of Q-dots was determined from X-Ray line broadening data using the Scherrer equation, and the estimated range was found to be 5-6 nm and 5-7 nm for CdS and (Cd,Mn)S quantum dots, respectively. As was observed in our earlier investigations [5, 24] that the calculated values of Q-dot size distribution, determined from the Scherrer equation, was systematically larger than that was observed and measured directly using the transmission electron microscopy. However, the values derived from two techniques were in good agreement and provided direct evidence.

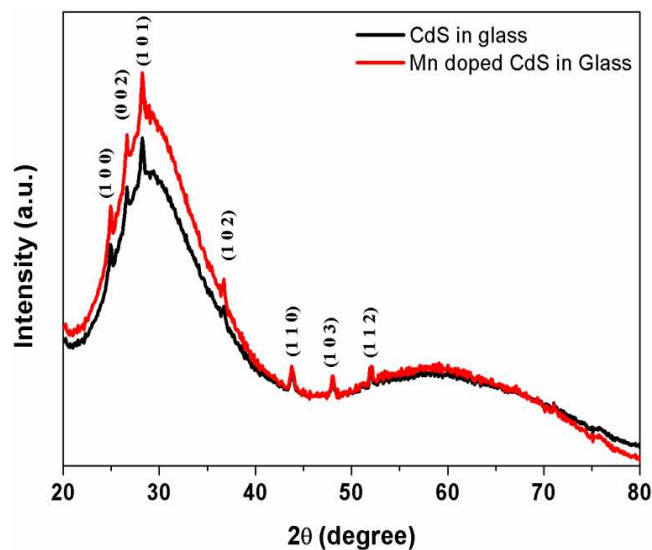


Fig.2: X-Ray powder diffraction pattern of CdS and Mn^{2+} -doped CdS in a silicate glass matrix heat treated at 600°C for 8 hours in air.

For more detailed microstructural properties of Q-dots formed after 8 hrs of annealing in air at 550°C and 600°C in the silicate glass matrix, the FE-TEM analysis was carried out and the images in Fig. 3 (a-h) show the morphological features, size distribution of Q-dots, selected area diffraction patterns (in insets) and lattice fringes of Q-dot particles. The SAED analysis in Fig. 3c and 3g also confirm that the Q-dot structures are of polycrystalline in nature and the doping of CdS Q-dots with Mn²⁺-ions does not change the morphological and phase constitution characteristics of Q-dots.

The FETEM micrographs in Fig. 3 (a - d) show nearly uniform spherical 3-4 nm and 4-5 nm CdS quantum dots, formed after 8 hours annealing at 550°C and 600°C for 8 hours, respectively. During early stage of annealing only 1-2 nm size crystallites are formed, as can be seen in Fig. 3 (a-b) and 3(e-f), respectively for CdS and Mn²⁺-doped CdS. From Fig. 3(c-d), the growth mechanism appears to be comparable with the Ostwald ripening phenomenon, via which the larger 5nm size CdS Q-dots form in glassy matrix. From both the selected area diffraction (SAD) and the lattice fringe analysis show that the measured values of d-spacing, 0.318nm and 0.317nm, corresponds to the (101) planes of hexagonal (JCPDF No. 077-2306) poly type of CdS and Mn²⁺-doped CdS solid solution phase, respectively.

From the FETEM analysis, the estimated size of Mn²⁺-doped CdS Q-dots, formed after annealing at 550°C and 600°C for 8 hours are 3-5 and 5-6 nm, respectively which compare reasonably well with the estimated values for CdS-doped Q-dots, and these values are in agreement within ±10%. Since, the ionic radius of Mn²⁺ (low spin radius=81 pm, high spin radius= 97pm) is smaller than that for Cd²⁺ at 109 pm, the lattice parameters is unlikely change significantly, considering that the maximum doping level of Mn²⁺ in CdS quantum dots may not be exceeding beyond 15 ion percent, when compared with the starting doping concentration of Cd_{0.844}Mn_{0.166}S. The glass transition temperature of host silicate glass is ~546°C, above which the QD-containing samples were annealed and then slowly cooled down to room temperature. Since, the ionic radii of Mn²⁺ and Cd²⁺ are comparable, it is apparent that there is no clear evidence from TEM for nano-scale CdS-MnS solid solution phase decomposition, arising as a result of heat treatment above T_g. Also, the crystal structures of CdS and MnS are based on zinc blend/wurtzite and rock salt, respectively, in which the crystallographic habit planes (101) may be

shared for promoting either isotropic or unidirectional growth on quantum scale, depending on the atomic packaging density of the dominating growth plane. However, the apparent growth in the 550-600°C is slow due to the high viscosity of matrix glass (10^6 - 10^7 Pa.s). Note that the amorphous silicate network does not offer any preferential growth direction for the nucleating CdS (with and without MnS) phase, thereby forcing the Q-dots to grow isotropically.

The ionic radius of S^{2-} anion is 170 pm, which means that the average distance between two sulphur anions (S^{2-}) will be no more than 340 pm. Assuming that CdS and MnS are thermodynamically stable at the silicate glass melting temperature, these two sulphides with over 270 pm cation (Mn^{2+}, Cd^{2+})-anion (S^{2-}) distance might be virtually insoluble in the silicate matrix with less than 175 pm ($Si^{4+}-O^{2-}$) bond distance. This is because for overall stability of silicate glass matrix, the soluble species must have comparable bond lengths for being accommodated within the silicate matrix. The apparent disparity between the bond lengths between the silicate and chalcogenide crystallites is likely to force the CdS Q-dots to nucleate within the amorphous matrix, which is the driving force for promoting nucleation and growth during, leading to Oswald ripening [5, 24-25]. Above T_g , the thermal energy promotes ionic conductivity leading to formation of CdS and $Cd_{1-x}Mn_xS$ phases, as shown schematically in Fig. 4.

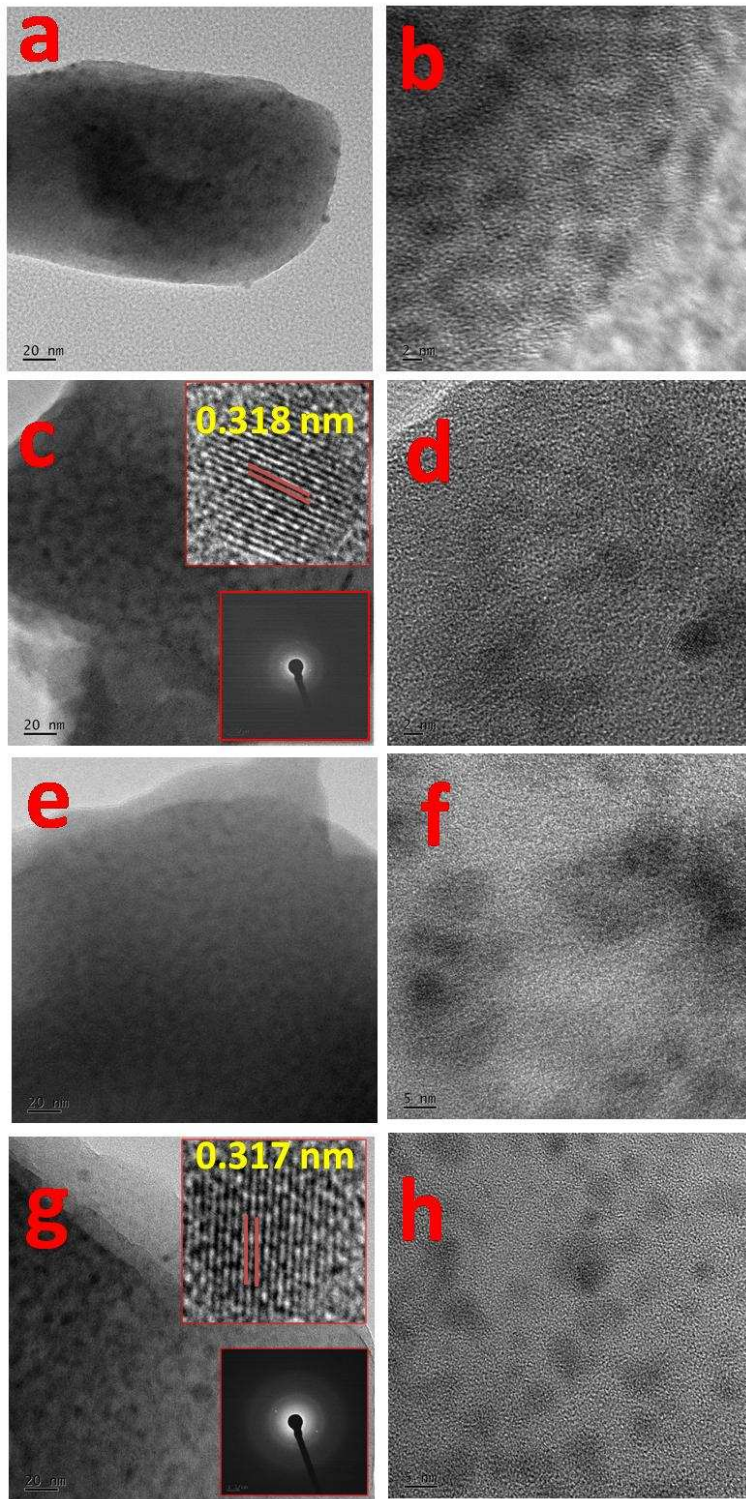


Fig. 3: TEM images of QDs formed via isothermal heat treatment conditions in a silicate glass matrix: (a,b) held at 550°C for CdS QD, (c,d) at 600°C for CdS QD, (e,f) Mn²⁺-doped CdS formed at 550°C and (g,h) formed at 600°C.

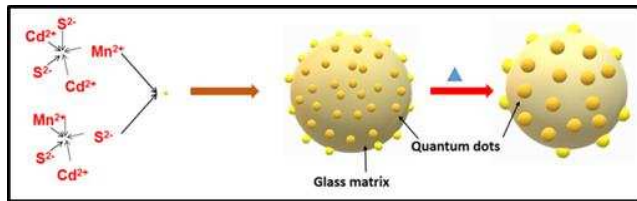


Fig. 4: Schematic representation of growth of Mn^{2+} -doped CdS in glass matrix

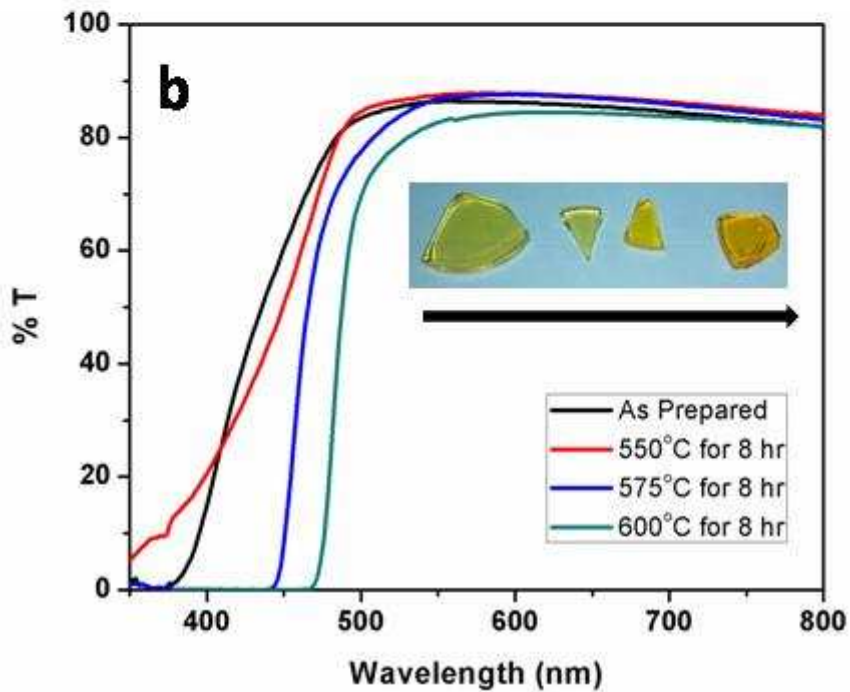
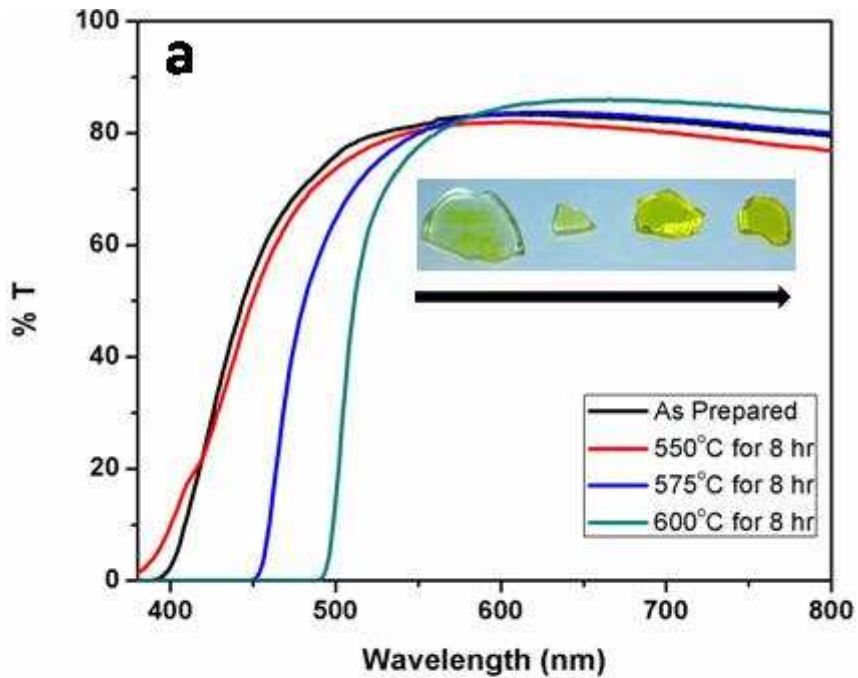


Fig. 5: Optical transmittances spectra for CdS (a) and Mn^{2+} -doped CdS (b) in glass.

Fig. 5a are 5b depict the UV-visible optical transmission spectra for CdS and Mn²⁺-doped CdS containing Q-dots, respectively. The corresponding Tauc plots are shown in Fig. ESI-II A&B. We conclude from the spectroscopic studies that:

(i) By increasing the heat treatment temperature from 550°C to 600°C, the size of QDs increase, resulting in the red shift of the electronic bandgap edge from 2.88eV to 2.51eV in Fig. 5a in the CdS-containing glass (see also ESI-IIA). The corresponding shift in Fig. 5b in the band edge for Mn²⁺-doped CdS QDs is from 2.88eV to 2.55eV (see also ESI-II B).

(ii) The incorporation of Mn²⁺-ions in CdS lattice blue shifts the band edge in the annealed glasses.

iii) The band edges of annealed glass samples at 550°C in Fig. 5a and 5b are not as sharply defined as that in the as-cast and annealed glasses above 550°C. This apparent difference is quite distinct in CdS- and Mn²⁺-doped CdS QDs samples, with a specific presence of absorption bands below 420nm. The change in the slope of the band edge at 550°C clearly confirms a distribution of QD states in the glass matrix which may be nucleating at sub-nano meter scale. Above 575°C, the average size of QDs increases with increasing temperature, under this condition the states in quantum dots become more sharply defined than the glass samples annealed below 575°C.

The average Q-dot size distribution was calculated from the experimentally measured absorption edge by using the Brus equation below [24-26]:

$$E_{\text{QD}} = E_{\text{bulk}} + \frac{\hbar^2 \pi^2}{8r^2} \left[\frac{1}{m_e^*} + \frac{1}{m_h^*} \right] - \frac{1.8e^2}{4\pi r \epsilon_0 \epsilon_{\text{CdS}}} \quad (1);$$

where E_{QD} and E_{bulk} designate the band gap of the quantum dots and bulk CdS, m_e^* and m_h^* are effective masses of electron and hole, and ϵ_0 and ϵ_{CdS} are the dielectric constants of vacuum and CdS, respectively. The table 1 shows the calculated QD size from the Brus model which compares reasonably with the size distribution data, determined using the TEM and XRD analyses.

Table 1 Comparison of average size of quantum dots using the Brus model [24-26].

Glass	Heat treatment temperature	Band gap (eV)	Calculated QD size (nm)
CdS-glass	Without Heat Treatment	2.88	2.24
	550°C held for 8 hours	2.79	2.50
	575°C held for 8 hours	2.64	3.20
	600°C held for 8 hours	2.51	4.69
Mn ²⁺ doped CdS-glass	Without Heat Treatment	2.88	2.24
	550°C held for 8 hours	2.75	2.63
	575°C held for 8 hours	2.68	2.94
	600°C held for 8 hours	2.55	4.01

Fig. 6(a and b) compare the room temperature photoluminescence (PL) of CdS and Mn²⁺-doped CdS Q-dots in the silicate glass matrix, annealed between 550°C and 600°C. The excitation wavelength for room temperature PL was 420nm. In case of Mn²⁺-doped CdS Q-dot glass, the colour changes as a result of heat treatment between 550°C and 600°C, and the consequential colour changes are compared in Fig.6 (a1, a2, b1, b2). For visualising fluorescence in bulk glass samples, we used 322 nm UV source as shown in Fig.6 (a2 and b2). The Fig.6a compares the PL spectra for CdS quantum dots in glass matrix which shows that the emission peak, centred at 648nm, shifts to longer wavelength i.e. 684nm when the annealing temperature increased from 550°C to 600°C. Such a temperature dependent PL emissions signifies the quantum confinement of CdS because average QD size increases with heat treatment which ultimately the red shifts the emission band. Also, there is an increase in the full width of half-maximum (FWHM) of the peak with increasing heat treatment of glass. However, above 550°C, the change in the shape of PL peak and FWHM is almost negligible. The apparent change in the FWHM corresponds to a distribution of inhomogeneous broadening of the contributing electronic states present in the Q-dots.

In the literature, there appears to be two different models for explaining the PL in the II-VI sulphur based Q-dots and these are attributed to the bound exciton emission of QDs as well as the electron-hole recombination of bulk like nano-crystallites (E_{ex}) and energetically different $V_{Cd}-V_S$ di-vacancies (E_I

and E_2) [26]. The second model, based on inter band pumping, is explained in Fig.6 [17,27,28]. For CdS Q-dot containing glass samples including as casted and heat treated (550°C - 600°C), the bound excitonic emission and electron-hole recombination model seems to be more plausible and such model may provide a broad band emission as shown in Fig.6a. Three emission peaks observed at 460, 516 and 648nm in the PL spectra of undoped CdS glass appear to have single Gaussian feature. However, the excitonic processes in undoped CdS Q-dots are perturbed by doping with Mn^{2+} ions due to the d-p electronic state interaction between Mn^{2+} and covalent S^{2-} becomes significant. Consequently, the changes in the corresponding excitonic and electron-hole pair interaction may be anticipated for energy transfer, which is explained in Fig.7. There is a strong evidence for energy level degeneration in Mn^{2+} -ions [24] of II-VI compounds, which may be influenced by the covalent bond structure (zinc blend and wurtzite) in the Q-dots and surface states of covalent bonds in the silicate glass matrix. The above PL related observations, compared in Fig. 6a and 6b, appear to be consistent with the Tanaka's energy model [24], corresponding to ${}^4\text{T}_{1-3}$ to ${}^6\text{A}_1$ for Mn^{2+} -ions in II-VI compounds, as shown in Fig. 7. Consequently, the line shape and the peak of emission of PL, as shown in Fig. 5b, are as expected from complex interactions between the p-states in Cd^{2+} , unoccupied d-states in Mn^{2+} and the p-states in S^{2-} anions, which will requires more detailed analysis, and is beyond the scope of this paper. The Mn^{2+} -ions apparently has a profound influence on the evolution of two high energy PL peaks in Fig. 6b at 541nm and 587nm. The main peak in the glass sample heat treated at 550°C is blue shifted to 620 nm with respect to the PL shown in Fig. 6a for CdS Q-dots. The peak at 587nm corresponds to a characteristic emission of Mn^{2+} ions ($E_{\text{Mn}} \sim 2.12$ eV) between the ${}^4\text{T}_1$ and ${}^6\text{A}_1$ levels in the Mn^{2+} doped CdS NPs [29, 30]. Furthermore, it is evident that the emission peak in the glass samples heat treated at 575°C and 600°C are shifted to much longer wavelengths in Mn^{2+} -doped CdS in Fig. 6b than in the undoped CdS in Fig. 6a. Based on the analysis of the Mn^{2+} energy level, a semi-quantitative energy level diagram for the transfer of energy from the Q-dots to the Mn^{2+} states is summarised in Fig. 7, which may be able to explain the reason for Stark splitting and energy transfer between the donor CdS states to acceptor Mn^{2+} -states.

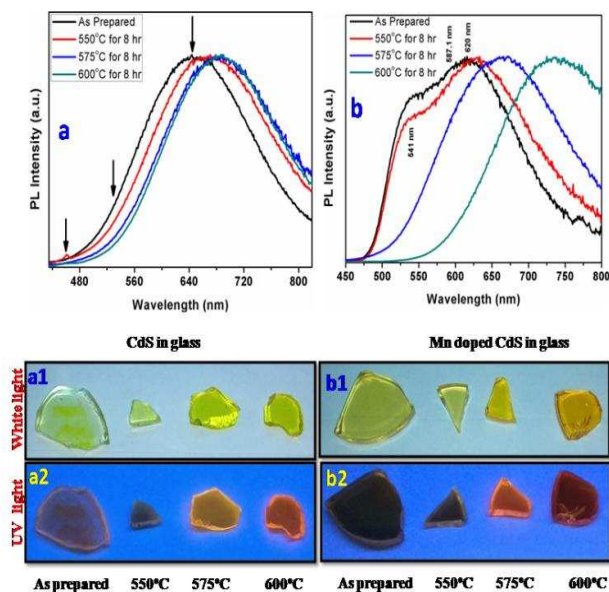


Fig. 6: Room temperature Photoluminescence spectra of CdS (a) and Mn doped CdS (b) and photograph of CdS glass (in white light a1 and UV light a2) and Mn doped CdS glass (in white light b1 and UV light b2). (Arrows in Fig. 5a shows the peak position of PL).

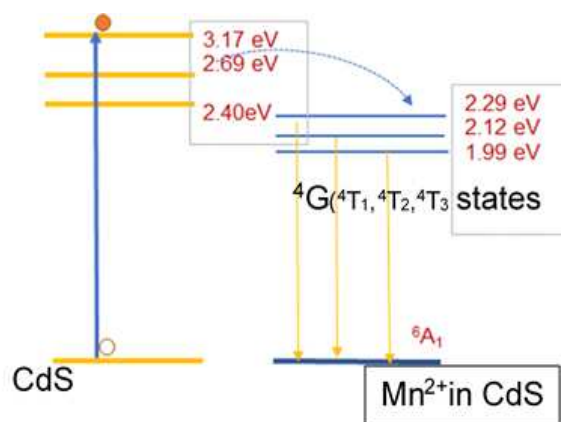


Fig. 7: Energy level representation energy transfer from CdS states to Mn^{2+} states (4G to 6A_1) in Mn^{2+} -doped CdS Q-dot glass [17].

The magneto-optical Faraday rotation (MOFR) investigations were performed for the CdS and Mn^{2+} doped CdS glasses at different wavelength. Fig.8 (a – h) show the linear increase in the value of MOFR with magnetic field. In the above figures, the variation of MOFR with Q-dot size, dependent on the heat treatment temperature is also apparent. The Verdet constants calculated from the measured Faraday rotation are shown in Fig. 9 and summarized in Table 2. There is a significant enhancement of FR in CdS and Mn^{2+} -doped CdS quantum dot glass samples with respect to host glass (See Fig. ESI IV and table ESI II in supporting information). It was observed that during quenching process, there is limited

crystallization of CdS and Mn²⁺-doped CdS quantum dots in glass matrix without annealing. The Verdet constant was calculated from the Faraday rotation angle. The calculated Verdet constants for the CdS and Mn doped CdS Q-dots in glass matrix were much greater than those for the host glass (see table 2). By comparing the values of Verdet constants of CdS and Mn²⁺-doped CdS Q-dots glass heat treated at 550°C for 8 hours, we found that values of Verdet constant nearly doubled from 6.2 to 12.0 degree/T-cm for Mn²⁺-doped CdS Q-dot glass. From table 2 and Fig. 8, it is evident that the Verdet constant decreases with increase in wavelength (λ).

When using 405 nm laser for MOFR characterisation in the CdS Q-dot glass, annealed at 550°C for 8 hours, the Verdet constant at 6.20 degree/T-cm was found to be 3.5 times larger than that in as-cast glass at 1.83 degree/T-cm. More significantly, in the Mn²⁺-doped CdS Q-dot glass heat treated at 550°C for 8 hours has 6.6 times larger value of Verdet constant (12.0 degree/T-cm) than the as-cast glass. The measured value of 12.0 degree/T-cm is also higher than that reported earlier for CdS-doped glasses [31].

From Table 2, it may be concluded that the measured values of Verdet constant is dependent on the annealing temperature, which determines the average size of Q-dots. At 405nm laser wavelength, the measured value of Verdet Constant is 2.60 degree/T-cm in the as cast CdS–glass structure, which increased to a value of 6.20 degree/T-cm after heat treatment at 550°C.

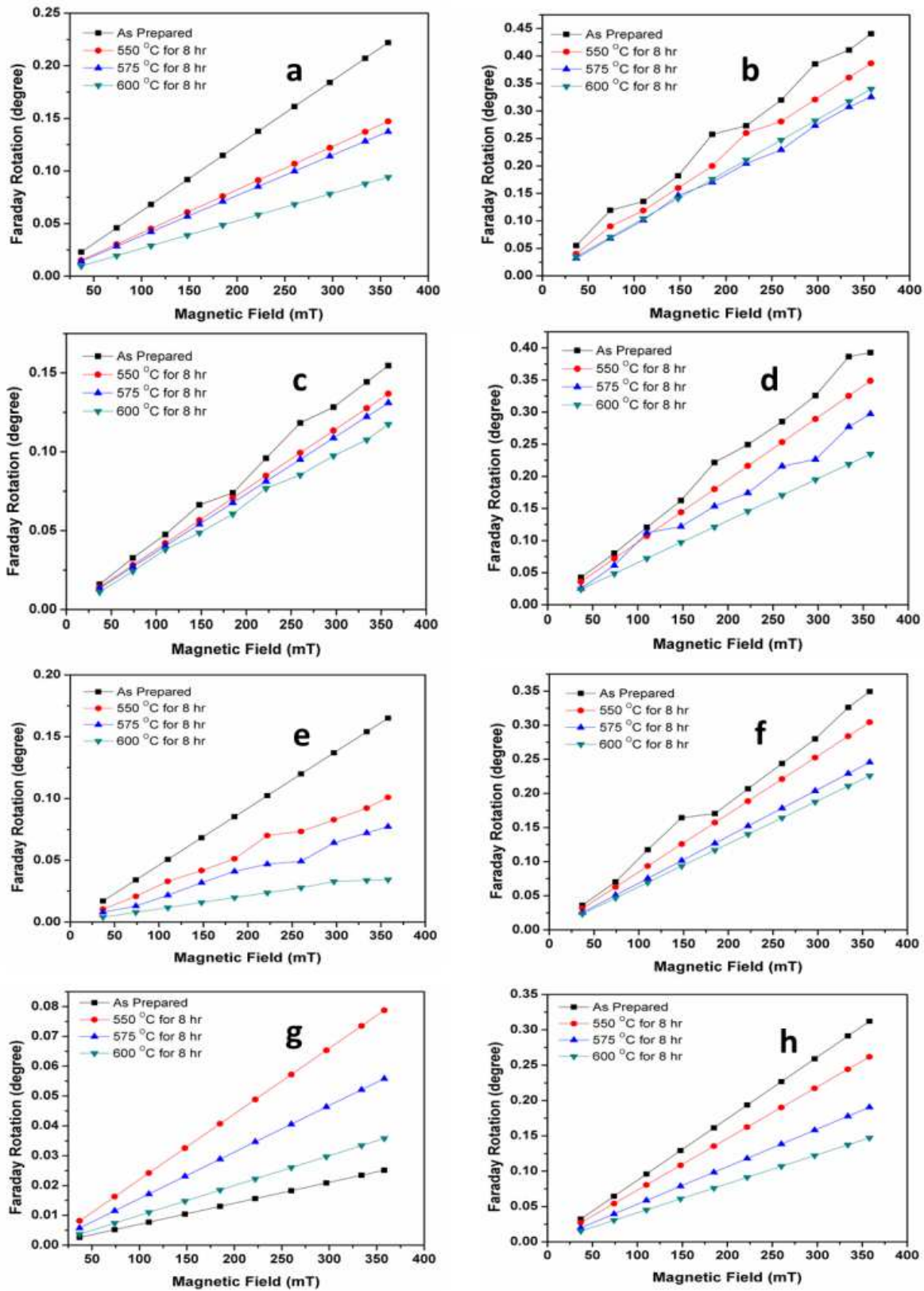


Fig. 8: Magnetic field dependent Faraday rotation measurements on CdS (a, c, e and g) and Mn doped CdS (b, d, f and h) for different wavelengths (405nm (a, b) 532nm (c, d), 635nm (e, f) and 670nm (g, h)).

Table 2 Summary of the measured Verdet constants for Q-dot CdS and Mn²⁺-doped CdS Glasses.

Verdet constants of glass treated (degree/T-cm)								
λ , nm	As prepared		550°C		575°C		600°C	
	CdS-glass	Mn doped CdS-glass	CdS-glass	Mn doped CdS-glass	CdS-glass	Mn doped CdS-glass	CdS-glass	Mn doped CdS-glass
405	2.60	9.50	6.20	12.0	4.11	10.70	3.84	9.70
532	3.26	6.56	4.34	11.2	3.82	9.74	3.66	8.01
635	0.99	6.31	4.81	9.46	2.79	8.50	2.17	6.86
670	1.40	8.72	2.20	7.31	1.56	5.32	1.00	4.11

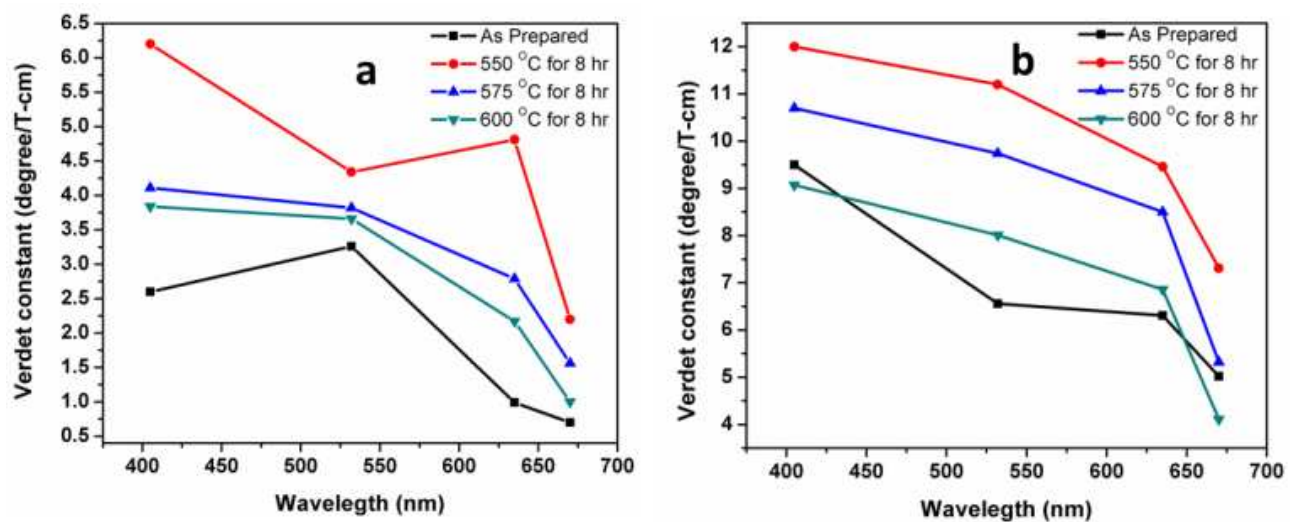


Fig. 9: Variation of Verdet constant against wavelength of laser source. a: CdS Q dots in glass, b: Mn²⁺-doped CdS Q-dots in glass.

The highest value of Verdet constant, 12.0 degree/T-cm, in the Mn²⁺-doped CdS Q-dot glass, annealed at 550°C decreased to 9.70 degree/T-cm when the annealing temperature was increased above 550°C. This is due to the fact that the temperature and time of annealing above the T_g of glass matrix controls the size distribution of Q-dots, and therefore the resonant bandgap for excitonic process via spin interaction in the confined geometry [32]. Similarly, the value of Verdet constant also decreases with increasing wavelength in the Mn²⁺-doped glasses.

It is well known that Faraday effect [27] is the rotation of the plane of polarization of linearly polarized light due to magnetic field induced circular birefringence in the material. The angle of Faraday rotation (θ_F , degree) is calculated by empirical formula as given below [28].

$$\theta_F = VBL \quad (2)$$

where V is Verdet constant, B (Tesla, T) is magnetic field strength in the direction of propagation of polarised light and L (cm) is the thickness of the sample. This effect arises as a result of the different indices of refraction for right ($n_{\sigma+}$) and left ($n_{\sigma-}$) circularly polarized light. The difference in the indices of refraction of right and left circularly polarized light ($n_{\sigma+} - n_{\sigma-}$) is proportional to the Faraday rotation θ_F , which is shown in equation (3) between θ_F and ($n_{\sigma+} - n_{\sigma-}$) [33].

$$\theta_F = \frac{\omega}{2c} (n_{\sigma+} - n_{\sigma-}) \quad (3)$$

The most significant distinction of diluted magnetic semiconductors (DMS) is the presence of magnetic exchange interactions [19, 34]. Amongst the DMS alloys ($A_{1-x}Mn_xB$) investigated, one can distinguish two types of spin interactions: a) the strong interaction between s, p-band and d- electrons of Mn and, b) the weaker d-d exchange interaction between neighbouring magnetic ions. Such exchange interactions between the 3d states in Mn²⁺-ions and the excitonic pair, created by the incident laser beam, induce cause Zeeman splitting [15], which is then enhanced by the applied magnetic field [35]. The magnitude of spin-state splitting,

ΔE_o , may be then determined as a difference of Zeeman components of circular polarization (E_d for $\sigma+$ and E_a for $\sigma-$), which for Mn²⁺-based DMS is described in equation 4:

$$\Delta E_o = E_d - E_a = N_o(\beta - \alpha)x \langle S_z \rangle \quad (4)$$

where N_o is the Avogadro number, $(\beta - \alpha)$ is exchange constant for the conduction and valence band respectively, $\langle S_z \rangle$ is the thermal average of the Mn²⁺ spins along the direction of the applied magnetic field. The magnitude of Zeeman splitting of absorption edge and exciton level in the Mn²⁺-doped CdS Q-dot medium yields a distribution of refractive indices for circularly polarized light [27]. Consequently, there is an enhancement in the Faraday rotation (θ_F), which can be expressed in one of the two forms:

$$\theta_F = \frac{L\sqrt{F_o}}{2\pi c} \frac{(\hbar\omega)^2}{(E_g^2 - (\hbar\omega)^2)^{\frac{3}{2}}} \Delta E_o \quad (5),$$

or

$$\theta_F = \frac{L\sqrt{F_o}}{2\pi c} \frac{(\hbar\omega)^2}{(E_g^2 - (\hbar\omega)^2)^{\frac{3}{2}}} N_o(\beta - \alpha)x \langle S_z \rangle \quad (6);$$

where, F_o is constant, L is thickness of sample, E_g is band gap and $\hbar\omega$ is photon energy of light. The equation (6) defines the relationship between the Faraday rotation, Zeeman splitting, energy gap and incident photon energy.

The observation of the highest value of Verdet constant of 12 degree/T-cm in the Mn²⁺-doped CdS containing Q-dot is the result of spin-state resonance with the incident photon at 405 nm. As the wavelength increases the spin-resonance condition weakens and, the magnitude of Verdet constant decreases, which is why the measured values of V show such strong dependence on the annealing temperature of the glass. The prima facie observations also show that the Verdet constant is also larger for smaller quantum dot size than that for the larger Q-dot size, which implies that by optimizing the Q-dot size for reducing the scattering loss in the medium, there is an opportunity for engineering M-O light waveguide devices.

4 Conclusions

We have successfully demonstrated the growth of CdS and Mn²⁺ doped CdS Q dots in a glass matrix. The spectroscopic and microstructural investigations showed a variation in band gap due to Mn²⁺-ion doping.

The data for the range of size distributions of Q-dots of CdS and Mn²⁺-doped CdS, determined using the FE-TEM, X-ray diffraction line broadening and Bohr radius estimation, are in agreement with the Brus model. As shown Table 1, these values range between 2.24nm to 4.64 nm and 2.24 to 4.01nm, respectively, for CdS and Mn²⁺-doped CdS glass Q-dot glasses, respectively. The average Q-dot size distribution decreases in the Mn²⁺-doped Q-dot, compared with the undoped CdS Q-dot for identical heat treatment conditions.

The photoluminescence spectra in the 430-800nm show distinct features of interaction between the excitonic pair in CdS with the spin-states in Mn²⁺, the emission peak broadening occurs more in Mn²⁺-doped CdS glass than in the undoped CdS glass.

The Faraday rotation measurements at different wavelengths of lasers in the visible range demonstrate strong influence of Mn²⁺ ions spin-state resonance, which is dependent on the lower size of the Q-dots. The highest Verdet constant (12 degree/T-cm) observed in such a glassy host, which might be useful for engineering waveguide based Faraday rotation device.

Acknowledgments

The research is financially supported by Ministry of Electronics and Information Technology (MeitY), Government of India, New Delhi and the Royal Society (London) funded International Collaboration between C-MET, Pune, India and University of Leeds, UK. Authors acknowledge this support as well as thankful to C-MET for providing all facilities.

References

- [1] N. O. Dantas, R. S. Silva, F. Pelegrini, and G. E. Marques, Morphology in semimagnetic $\text{Pb}_{1-x}\text{Mn}_x\text{Se}$ nanocrystals: Thermal annealing effects, *Appl. Phys. Lett.* 94 (2009) 263103-263105.
- [2] K. Miyamoto, K. Isai, M. Suwa, H. Watarai, Effective Transition Probability for the Faraday Effect of Lanthanide(III) Ion Solutions, *J. Am. Chem. Soc.* 131 (2009) 6328-6329.
- [3] D. J. Norris, A. L. Efros, S. C. Erwin, Doped Nanocrystals, *Science* 319 (2008) 1776-1779.
- [4] A. Aboulaich, L. Balan, J. Ghanbaja, G. Medjahdi, C. Merlin, R. Schneider, Aqueous route to biocompatible ZnSe: Mn/ZnO core/shell quantum dots using 1-thioglycerol as stabilizer, *Chem. Mater.* 23 (2011) 3706-3713.
- [5] R. P. Panmand, G. Kumar, S. M. Mahajan, M. V. Kulkarni, B. B. Kale, A. P. Gosavi, Novel and stable Mn^{2+} - Bi_2S_3 quantum dots–glass system with giant magneto optical Faraday rotations, *J. Mater. Chem.C* 1 (2013) 1203-1210.
- [6] W. Crossley, R. Cooper, J. Page, R. Van Staple, Faraday rotation in rare-earth iron garnets, *Phys. Rev.* 181 (1969) 896-905.
- [7] T. Hayakawa, M. Nogami, N. Nishi, N. Sawanobori, Faraday Rotation Effect of Highly $\text{Tb}_2\text{O}_3/\text{Dy}_2\text{O}_3$ -Concentrated B_2O_3 - Ga_2O_3 - SiO_2 - P_2O_5 Glasses, *Chem. Mater.* 14 (2002) 3223-3225.
- [8] G. Gao, A. Winterstein-Beckmann, O. Surzhenko, C. Dubs, J. Dellith, M. A. Schmidt, L. Wondraczek, Faraday rotation and photoluminescence in heavily Tb^{3+} -doped GeO_2 - B_2O_3 - Al_2O_3 - Ga_2O_3 glasses for fiber-integrated magneto-optics, *Scientific Rep.* 5 (2015) 8942-8947.
- [9] I. Katakura, M. Tokunaga, A. Matsuo, K. Kawaguchi, K. Kindo, M. Hitomi, D. Akahoshi, H. Kuwahara, Development of high-speed polarizing imaging system for operation in high pulsed magnetic field, *J. Rev. Scientific Instruments* 81 (2010) 043701-043708.
- [10] R K. Sinha and Y Kalra, Design of optical waveguide polarizer using photonic band gap, *Opt. Exp.* 14 (2006) 10790-10794.
- [11] C. Koos, P. Vorreau, T. Vallaitis, P. Dumon, W. Bogaerts, R. Baets, B. Esembeson, I. Biaggio, T. Michinobu, F. Diederich, All-optical high-speed signal processing with silicon–organic hybrid slot waveguides, *Nat. Photon.* 3 (2009) 216-219.
- [12] I. Edelman, J. Kliava, Oxide glasses with magnetic nanoparticles: transparent magnets (Faraday rotation and electron magnetic resonance studies), *Phys. Stat. Solid.* 246 (2009) 2216-2231.
- [13] W. Li, K. Zou, M. Lu, B. Peng, W. Zhao, Faraday Glasses with a Large Size and High Performance, *Inter. J. Appl. Ceram. Techn.* 7 (2010) 369-374.
- [14] V. Fediv, A. Savchuk, V. Frasunyak, V. Makoviy, O. Savchuk, Magnetic and magneto-optical properties of CdS: Mn quantum dots in PVA matrix, *J. Physics: Conf. Ser.* 245 (2010) 012084 (3 pages).
- [15] J. K. Furdyna, Diluted magnetic semiconductors, *J. Appl. Phys.* 64 (1988) R29-64.

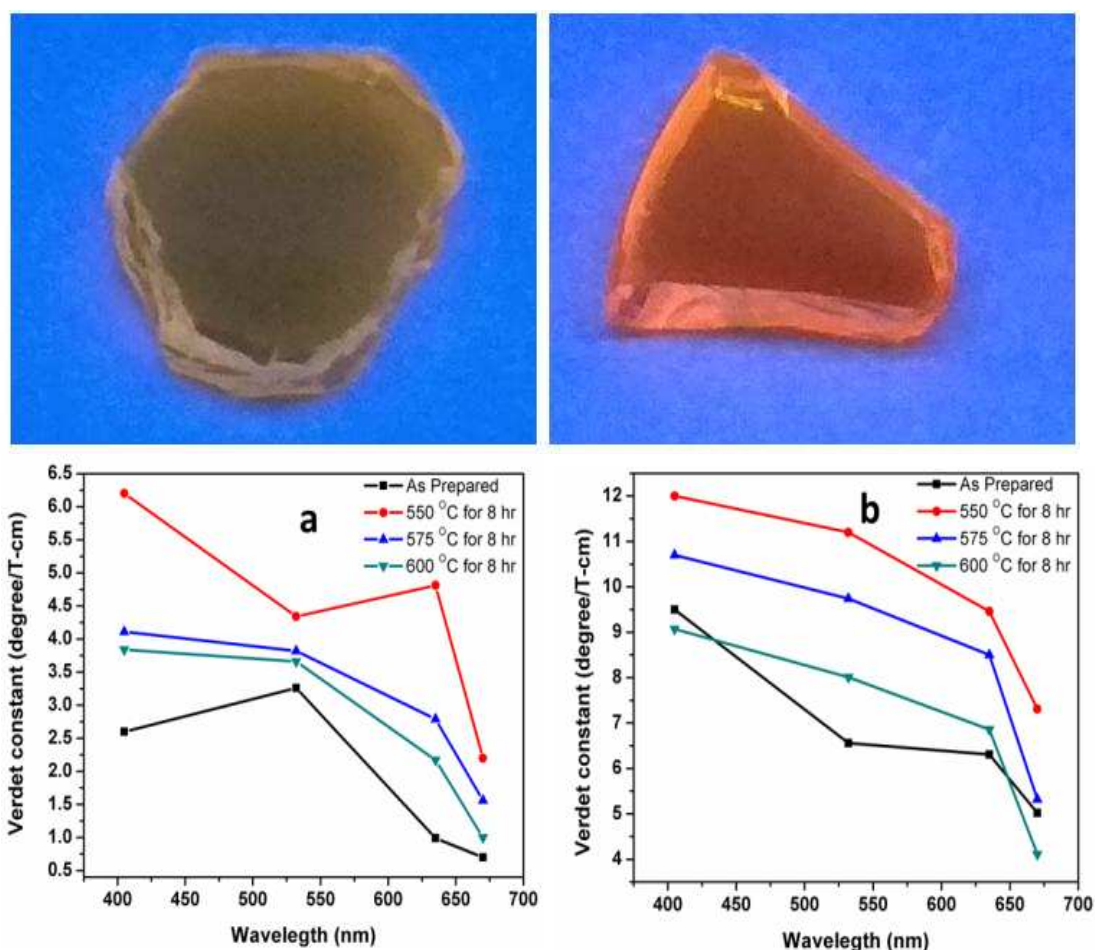
- [16] D. Cai, A. Neyer, R. Kuckuk, H. Heise, Optical absorption in transparent PDMS materials applied for multimode waveguides fabrication, *Opt. Mater.* 30 (2008) 1157-1161.
- [17] M. Tanaka, Photoluminescence properties of Mn^{2+} -doped II–VI semiconductor nanocrystals, *J. Lumin.* 100 (2002) 163-173.
- [18] R. Silva, P. Morais, E. Mosiniewicz-Szablewska, R. Cuevas, J. Campoy, F. Pelegrini, F. Qu, N. Dantas, Synthesis and magnetic characterization of $Pb_{1-x}Mn_xS$ nanocrystals in glass matrix, *Appl. Phys. Letts.* 90 (2007) 253114-253116.
- [19] N. O. Dantas, F. Qu, R. S. Silva, P. C. Morais, Anti-Stokes Photoluminescence in Nanocrystal Quantum Dots, *J. Phys. Chem.B.* 106 (2002) 7453-7457
- [20] A. Savchuk, S. Y. Paranchych, V. Frasunyak, V. Fediv, Y. V. Tanasyuk, Y. O. Kandyba, P. Nikitin, Optical and magneto-optical study of CdTe crystals doped with rare earth ions, *J. Mater. Sci.B.* 105 (2003) 161-164.
- [21] R. P. Panmand, G. Kumar, S. M. Mahajan, M. V. Kulkarni, D. Amalnerkar, B. B. Kale, S. W. Gosavi, Functionality of bismuth sulfide quantum dots/wires-glass nanocomposite as an optical current sensor with enhanced Verdet constant, *J. Appl. Phys.* 109 (2011) 033101-033108.
- [22] N. O. Dantas, G. L. Fernandes, O. Baffa, J. A. Gómez, A. C. A. Silva, Controlling Densities of Manganese Ions and Cadmium Vacancies in $Cd_{1-x}Mn_xTe$ Ultrasmall Quantum Dots in a Glass Matrix: x-Concentration and Thermal Annealing, *J. Phys. Chem. C*, 119 (2015) 17416-17420.
- [23] E. S. F. Neto, N. O. Dantas, S. A. Lourenço, Carrier dynamics in the luminescent states of $Cd_{1-x}Mn_xS$ nanoparticles: effects of temperature and x-concentration, *J. Phys. Chem. Chemical Phys.* 14 (2012) 1493-1501.
- [24] R. P. Panmand, G. Kumar, S. M. Mahajan, N. Shroff, B. B. Kale, S. W. Gosavi, Growth of Bi_2Te_3 quantum dots/rods in glass: a unique highly stable nanosystem with novel functionality for high performance magneto optical devices, *J. Phys. Chem. Chemical Phys.* 14 (2012) 16236-16242.
- [25] J. Nanda, S. Sapra, D. Sarma, N. Chandrasekharan, G. Hodes, Size-Selected Zinc Sulfide Nanocrystallites: Synthesis, Structure, and Optical Studies, *Chem. Mater.* 12 (2000) 1018-1024.
- [26] E. S. F. Neto, N. O. Dantas, N. M. B. Neto, I. Guedes, F. Chen, Control of luminescence emitted by $Cd_{1-x}Mn_xS$ nanocrystals in a glass matrix: x concentration and thermal annealing, *Nanotechnology* 22 (2011) 105709-105714.
- [27] A. I. Savchuk, M. P. Gavaleshko, A. M. Lyakhovich, P. I. Nikitin, Magneto-optical effects induced by exchange interaction in diluted magnetic semiconductors, *IEEE Trans. Magnetics* 29 (1993) 3399-3401.
- [28] H. Akamatsu, K. Fujita, S. Murai, K. Tanaka, Magneto-optical properties of transparent divalent iron phosphate glasses, *Appl. Phys Letts.* 92 (2008), 251908-251911.
- [29] M. A. Kamran, A. Majid, T. Alharbi, M. W. Iqbal, M. W. Amjad, G. Nabi, S. Zou, B. Zou, Large tunable luminescence by Mn(ii) aggregates in Mn-doped ZnS nanobelts, *J. Mater. Chem.C.* 5 (2017) 8749-8757.

- [30] E. S. F. Neto, N. O. Dantas, S. A. Lourenco, M. D. Teodoro, G. E. Marques, Magneto-optical properties of $\text{Cd}_{1-x}\text{Mn}_x\text{S}$ nanoparticles: influences of magnetic doping, Mn^{2+} ions localization, and quantum confinement, *Phys. Chem. Chemical Phys.* 14 (2012) 3248-3255.
- [31] P. R. Watekar, H. Yang, S. Ju, W.T. Han, CdSe Quantum Dots Doped Optical Fiber as a Remote Current Sensor, *Optics Exp.* 17 (2009) 3157-3163.
- [32] J. H. Kratzer, J. Schroeder, Magneto-optic properties of semiconductor quantum dots in glass composites, *J. Non-crystal. Sol.* 349 (2004) 299-308.
- [33] L. Luan, W. Jie, J. Zhang, P. Li, Faraday rotation in indium doped $\text{Cd}_{1-x}\text{Mn}_x\text{Te}$ single crystals, *Solid State Comm.* 149 (2009) 357-360.
- [34] J. Suyver, S. Wuister, J. Kelly, A. Meijerink, Luminescence of nanocrystalline ZnSe:Mn^{2+} , *J. Phys. Chem. Chemical Phys.* 2 (2000) 5445-5448.
- [35] H. Yin, C. Zhang, L. Liu, Y. Li, B. Tang, New Progress in Research on Faraday Magneto-optical Glass Containing Rare-earth, *Mater. Rev.* 22 (2008) 7.

Characterizations of Spectroscopic and Magneto-optical Faraday rotation in Mn^{2+} -doped CdS quantum dots (QDs) in a silicate glass

Shashikant Tekale, Rajendra P. Panmand, Krishna D. Daware, Suresh W. Gosavi, Animesh Jha and Bharat B. Kale

The control of quantum dots (QD) of hexagonal phase of CdS and Mn^{2+} -doped CdS in a silicate glass matrix is feasible via conventional glass fusion and annealing methods. The control of Q-dot structures in a silicate glass matrix offers opportunity for tailoring both the photoluminescence (PL) and magneto-optical properties which are characterized herein using the PL and Faraday magneto-optical measurements. Such glass based optically active materials are potentially suitable for pump isolators, polarization control in lasers and amplifiers, data encryption, and in magneto-optical current sensors.



Highlights for review

We demonstrate control of dimetal chalcogenide quantum dots (CdS and Mn²⁺-doped) in a silicate glass matrix, using post casting annealing process. The size distribution range (2-4.7 nm) of CdS and Mn²⁺ doped CdS QDs may be tuned by annealing in the 550°C and 650°C range. The photoluminescence spectra change as a result of change in the local field due to spin-state and excitonic state interaction. Such interaction also lead to a significant enhancement in the Verdet constant 6.2 to 12.0 deg/Tcm in CdS QD glass to Mn²⁺-doped Q-dot glass materials for engineering optical waveguides for polarization controlling magento-optical devices, requiring sub-Tesla field.